TURBULENCE STRUCTURE AND TRANSFER CHARACTERISTICS IN THE SURFACE LAYER OF HEIFE GOBI AREA *

Wang Jiemin(王介民), *Liu Xiaohu* (刘晓虎) and *Ma Yaoming* (马耀明)

Lanzhou Institute of Plateau Atmospheric Physics, Academia Sinica, Lanzhou

Received December 17, 1990

ABSTRACT

Based on the HEIFE 1988 and 1990 pilot observations, an analysis on the turbulence structure of Gobi surface layer, mainly on the similarity formulations of wind and temperature variances, the spectra and cospectra characteristics, is presented. The phenomenon of downward water vapor flux over Gobi desert in daytime is confirmed in both observations, this and the well-known 'oasis effect' are two sides of a local mesoscale circulation.

Key words: HEIFE, Gobi, surface layer, turbulence structure, turbulence transfer

I. INTRODUCTION

In the 'atmosphere–land surface interaction processes experiment at Heihe River Basin (HEIFE)' there are five stations located in the oasis, Gobi, and desert area. The surface difference of these areas causes apparent differences in their boundary layer structures and in characteristics of turbulence transfer of energy, water vapor, etc. The study of these characteristics and their interrelation is a special feature of HEIFE, when compared with similar experiments carried out in other countries. A bird's–eye view to the whole experimental region is mainly a large area of Gobi and / or desert, with some oases dispersed along the river and irrigation canals. The surface state of the oases is complicated due to the network of cropland and windbreak trees and the scattered residential areas. Comparatively, the Gobi surface is simpler, and it is easier to arrange observational study in the first stage. So the HEIFE Pilot Observation (POP) in 1988 and Pilot Intensive Observation (PIOP) in 1990 were all carried out at Gobi Station. In addition to testing the whole observation system and methodology, we have made a preliminary study of the turbulence transfer characteristics over Gobi desert based on the POP data. A peculiar phenomenon of downward water vapor flux over Gobi desert in the daytime was noticed (Wang et al., 1990). Here we present a further analysis on both POP and PIOP, mainly on the characteristics of turbulence structure and turbulence transfer in the Gobi surface layer.

The turbulence transfer of momentum, heat and water vapor is a fundamental aspect in the investigation of atmosphere–surface interaction, and it is closely related to the structure of surface layer even the whole boundary layer. For an atmospheric entity C its vertical flux F can be evaluated through measuring time series $C(t)$ and the vertical velocity $W(t)$, and doing

* The HEIFE program is supported by National Natural Science Foundation of China, the Chinese Academy of Sciences, and the Special Committee for WCRP of the Geodesy Council, Japanese Ministry of Education, Science and Culture.

multiplication and average,

$$F = \overline{WC} = \overline{w'c'} \ , \tag{1}$$

where w' and c' are the fluctuation parts of $W(t)$ and $C(t)$ respectively. This is equivalent to integration of the cospectrum of $\overline{w'c'}$, $C_o(f)$, over frequency (f) domain,

$$\overline{w'c'} = \int_0^\infty C_o(f)df \ . \tag{2}$$

According to surface layer structure analysis the energy containing eddies are the carrier of various turbulence transportation. A correct calculation of flux through (1) or (2) requires that the measured time series of $W(t)$ and $C(t)$ keep fidelity in both amplitude and phase in the whole energy containing region. Referring to turbulence spectra characteristics this corresponds to a requirement of the frequency response range in the process of measurement and averaging:

$$10^{-3} \leqslant \frac{fz}{\bar{u}} \leqslant 5\text{—}10 \ , \tag{3}$$

where f is natural frequency, z measuring height, and $\bar{u}$ the mean wind speed.

Calculating flux through (1) or (2) is the so–called eddy correlation method. Besides some conditions such as stationarity and horizontally homogeneous surface there are no essential assumptions. Therefore where accuracy in the measurements is an important concern, this method is an only clear choice; However, the instrument sensors are relatively expensive and often require trained personal to operate. There are also some difficulties in the management of huge amount of turbulence data in common field conditions. Based on recent advances in microcomputer–control technology, a low cost, real time turbulence data acquisition and processing system has been developed and successfully operated in HEIFE experiment. The specific advantages of this system are a nearly immediate access to the measured and calculated quantities, better quality control of the data, and the ability for investigators to determine quickly if correlations observed are statistically significant.

II. EXPERIMENT AND DATA

As the site and instrumentation are described in detail in Wang et al. (1990), only a further brief introduction is given here. The HEIFE Gobi Station (100°06′E, 39°09′N, 1480m ASL) is situated in the south part of Heihe River Basin, approximately 1.5—2 km to the south of Linze oasis and 30 km to the north of Qilian Mountain. The surface is flat and open, particularly on the south, and consists of coarse sand grains and small pebbles with very sparse scrup vegetation. Its geomorphic feature is consistent with conditions all along the south part of the basin. Fig. 1 shows a land use map around the station.

The HEIFE POP was conducted mainly in the September of 1988. Besides a 20 m profile tower (mean wind and temperature) and radiation measurements, a set of turbulence sensors, including a three–dimensional sonic anemo–thermometer (Kaijo–Denki, DAT–300), a 12μm tungsten wire thermometer, and a fine wire (80 μm) thermocouple psychrometer (Kaijo–Denki, PY–100), have been used for eddy–correlation measurements. In the PIOP, carried out in August, 1990, two sets of turbulence data acquisition system similar to that of 1988, including a Lyman–Alpha hygrometer, have been operated. Besides, a tethered–sonde system and two versions of acoustic sondar were used simultaneously in probing the boundary layer structure.

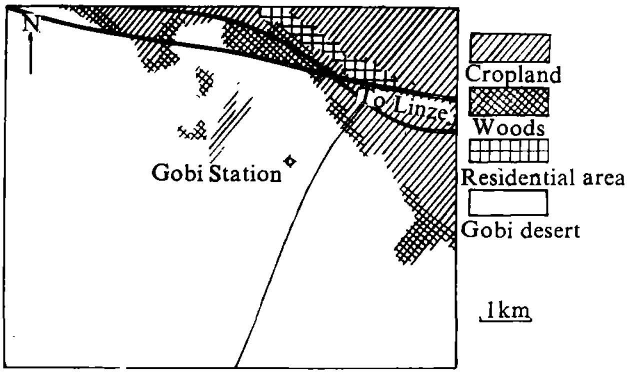

Fig. 1. Land use map around the HEIFE Gobi Station.

Sonic anemo–thermometer has been the essential instrument in the direct measurement of turbulence fluxes. In order to extend data utility the sonic probe was carefully adjusted in most hours so that the cross angle of 120–degrees between the horizontal components faces the prevailing wind direction. The tilt angle of its vertical component was also checked constantly. Low–pass active filters (DC to 10 Hz) were used before the data digitization to reduce higher frequency noise. A proper method was adopted to correct the probe 'shadow effect' in data processing (Grant and Watkins, 1989).

The data acquisition and processing were performed with an I. M personal computer. In most cases data were sampled at 10 Hz during 30 to 45–minute runs. With a well–done software the data could be processed in about 10 minutes after each run, including eddy–correlation calculations and spectral analysis, with a paper printing or data file output of the concerned statistical quantities, such as means, variances, correlations, stability parameter, momentum, heat, and water vapor fluxes, and the power spectra of wind components, temperature, specific humidity, and the cospectra of momentum and heat flux, etc. Some proper treatments for the original time series, such as despiking, detrending, and some corrections to the sensors (including a time constant correction for the thermocouple psychrometer (Tsukamoto, 1986)) were also correspondently considered in the data processing procedure.

As checked by the analyzed results, the turbulence data collected in both POP and PIOP are of high quality. In the following sections an investigation on the turbulence structure and turbulence transfer characteristics is presented, mainly on a similarity analysis of the variances, the characteristics of turbulence spectra and cospectra, and a re–examination of the phenomenon of downward water vapor flux observed over Gobi desert in daytime. About 88 runs in POP and 135 runs in PIOP are selected in this analysis, in which various air stabilities and wind directions are included. Some runs are discarded according to the following criteria:

(1) The mean wind azimuth deviation referring to the sonic coordinate system is larger than 45 degrees;

(2) Wind speed is lower than 1 m / s and normally with a very low value of $|\overline{u'w'}|$ even a positive $\overline{u'w'}$ (where u' is along–wind fluctuation). These occurred mostly in the stability transient hours of morning and late afternoon, normally with an apparent nonstationarity.

III. SIMILARITY ANALYSIS OF VARIANCES

According to Monin–Obukhov (M–O) hypothesis, various statistics of atmospheric parameters, such as gradients, variances, and covariances, when normalized by appropriate powers of the scaling velocity u_* and scaling temperature T_*, become universal function of z/L. As normally defined in the surface layer,

$$u_* = (\overline{-u'w'}) \ , \tag{4}$$

$$T_* = \frac{(\overline{-w'\theta'})}{u_*} \ , \tag{5}$$

$$\frac{z}{L} = -\frac{(g/T)(\overline{w'\theta'})}{u_*^3/kz} \ , \tag{6}$$

where L is M–O length, T mean temperature, θ' potential temperature fluctuation, K Von Karman constant. The relevant non–dimensional forms are mainly

$$\frac{kz}{u_*}\frac{\partial \bar{u}}{\partial z} = \varphi_m(\frac{z}{L}) \ , \quad \text{(wind shear)} \tag{7}$$

$$\frac{kz}{T_*}\frac{\partial \bar{\theta}}{\partial z} = \varphi_h(\frac{z}{L}) \ , \quad \text{(temperature gradient)} \tag{8}$$

$$\frac{kz\varepsilon}{u_*^3} = \varphi_\varepsilon(\frac{z}{L}) \ , \quad \text{(dissipation of turbulent kinetic energy)} \tag{9}$$

$$\frac{\sigma_w}{u_*} = \varphi_w(\frac{z}{L}) \ , \quad \text{(standard deviation of } w'\text{)} \tag{10}$$

$$\frac{\sigma_\theta}{|T_*|} = \varphi_\theta(\frac{z}{L}) \ . \quad \text{(standard deviation of } \theta'\text{)} \tag{11}$$

The forms of universal function φ_w and φ_θ have been concerned in many studies since based on these relationships th shear stress ($\tau = \rho(\overline{-u'w'})$) and sensible heat flux ($H = \rho C_p \overline{w'\theta'}$) can be rather easily evaluated through measurements of the variances of vertical velocity and temperature. A free convection asymptotic analysis shows that $\sigma_w/u_* \propto (-z/L)^{1/3}$ and $\sigma_\theta/|T_*| \propto (-z/L)^{-1/3}$; and based on observation data the propotional constants are 1.90 and 1.96 respectively (Wyngaard, 1973). In addition, at neutral stratification, σ_w/u_* and σ_θ/u_* should become constant. Panofsky and Dutton (1984) summarized some observations in uniform terrain and presented a mean value, $\sigma_w/u_* = 1.25$. They also recommended an empirical form for unstable situation:

$$\frac{\sigma_w}{u_*} = \varphi_w = 1.25(1 - 3\frac{z}{L})^{1/3} \ , \qquad (z/L \leqslant 0) \tag{12}$$

which is commonly referred in the literatures. In stable air considering the low accuracy in determining σ_w and u_* and other factors, Panofsky and Dutton still recommended σ_w/u_* being a constant 1.25, i.e. its neutral state value.

For φ_θ there are not so many references. Based on mixing length concept Panofsky and Dutton (1984) introduced a formula for unstable and neutral stratification,

$$\varphi_\theta = c\varphi_h = c(1-16\frac{z}{L})^{-1/2}, \qquad (z/L \leqslant 0) \tag{13}$$

where $c \approx 5$ when compared with some observation data. However, this form is inconsistent with the asymptotic analysis of free convection.

Figs. 2 and 3 show the variations of σ_w / u_* and $\sigma_\theta / |T_*|$ versus stability obtained from HEIFE observations at Gobi Station. The data distribution for both POP and PIOP are quite similar so only the latter is presented. Compared to some observations in the literature, data points in Figs. 2 and 3 show a less scatter, particularly, in unstable side. It is apparent that under $z/L<-0.35$ both σ_w / u_w and $\sigma_\theta / |T_*|$ are in good agreement with the predictions of free convection. Panofsky–Dutton formula, Eq. (12) is also plotted in Fig. 2 (dashed curve), which is obviously higher than our observations. Particularly in the range of $-0.1<z/L<0$ the calculated values of Eq. (12) are 5—10% larger. Whereas in the stable side, the observed data points of σ_w / u_* show a little increasing with stability, as confirmed by some other experiments, for example the recent results by Shaw and Hacker (1990). The solid curve in Fig. 2 represents a best fit of the present data, which can be summarized by

$$\frac{\sigma_w}{u_*} = \varphi_w = \begin{cases} 1.90(-z/L)^{1/3}, & (z/L \leqslant 0.35) \\ 1.14(1-1.5z/L)^{1/3}, & (-0.35<z/L \leqslant 0) \\ 1.14(1+0.6z/L). & (z/L>0) \end{cases} \tag{14}$$

For neutral stratification the present data show that $\sigma_w / u_* = 1.14$, a constant smaller than the commonly recognized Panofsky's value 1.25. In fact, the latter was a simple average of about 10 observations conducted over both sea and land. The individual values of those observations were ranged from 1.10 to 1.40. Recently, based on an experiment in Lovsta, Hogstrom (1990) indicates that the near–neutral value of σ_w / u_* increases with height above ground (several second and third moments, such as $\overline{w'^2}$, $\overline{u'^2 w'}$ and $\overline{v'^2 w'}$ are not, as expected, constant in the surface layer, but very logarithmically with height). In Lovsta data the mean values of σ_w / u_* at 3, 6, and 14 meters were 1.14, 1.23, and 1.33 respectively. Hogstrom found that this is due to the so–called 'inactive' turbulence. The present result of HEIFE Gobi Station (with mounting height $z=2.45$ m) was quite consistent with that of Lovsta 3 m data.

The best fit function form for $\sigma_\theta / |T_*|$ in the present study is

$$\frac{\sigma_\theta}{|T_*|} = \varphi_\theta = \begin{cases} 0.96(-z/L)^{-1/3}, & (z/L \leqslant -0.30) \\ 3.0(1-25z/L)^{-1/3}, & (-0.30<z/L \leqslant 0) \\ 3.0. & (z/L>0) \end{cases} \tag{15}$$

As in many other experiments the data points in near neutral and stable stratification show a larger scatter; It is difficult to make a proper simulation. However the recent result by Shao and Hacker (1990), derived on a local similarity analysis, is quite similar to Eq.(15).

A similar analysis for the along–wind and cross–wind components was also conducted. The non–dimensional values of σ_u / u_* and σ_v / u_* are about 2.65 and 2.22 respectively at near neutral conditions, which are very near the result of Panofsk and Dutton. Along with the increasing of instability (when $z/L<-0.1$), the data points show a very large scatter; The surface similarity is no longer valid. This is due to the influence of boundary layer structure of higher altitude, and is consistent with the results of turbulence spectral analysis presented in the next section.

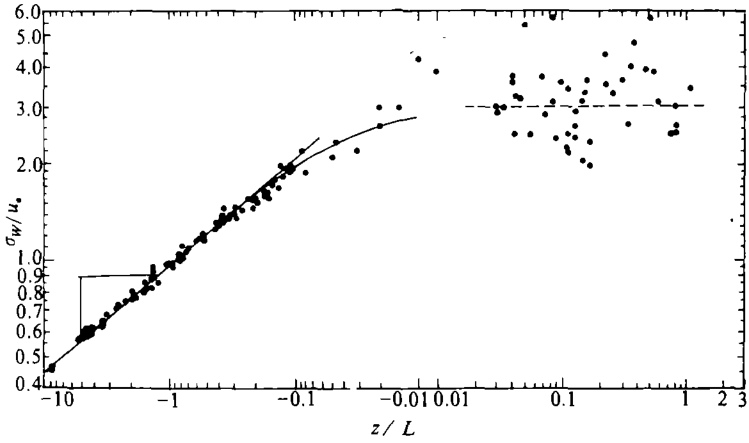

Fig. 2. Variations of σ_w / u_* versus stability. Dashed curve is the simulation of Panofsky and Dutton (Eq. 12). Slope 1 / 3 line is the free convection asymptotic. The solid line is the best fit of this experiment (Eq.14).

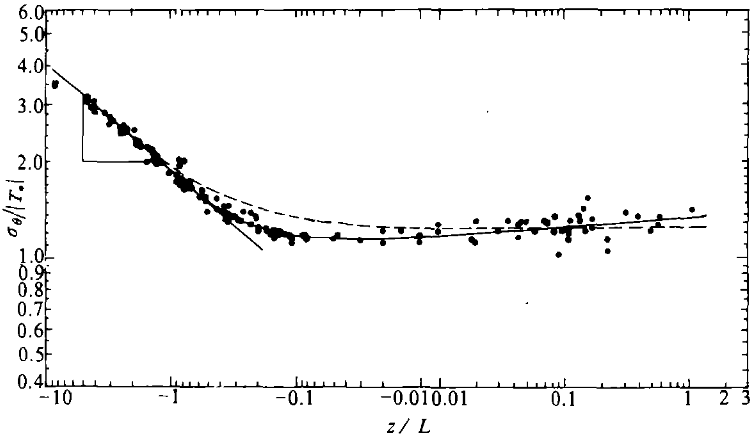

Fig. 3. Variations of $\sigma_\theta / |T_*|$ versus stability. Solid curve is the best fitted line of this experiment (Eq. 15). (Data points in stable part are very scattered, the constant value shown by dashed line is for reference).

IV. BASIC CHARACTERISTICS OF TURBULENCE SPECTRA

Figs. 4—7 show the power spectra of wind components w, u, v and temperature T of five runs at different stabilities in the HEIFE PIOP. The abscissa is the commonly–used reduced frequency $n = (f\ z) / \bar{u}$, the ordinate is the normalized spectra using Kaimal's scheme (Kaimal et al., 1972). The basic form of u–spectrum, for example, in the inertial subrange,

$$F_u(k_1) = \alpha_u \varepsilon^{2/3} k_1^{-5/3}, \tag{16}$$

(where k_1 is wavenumber in the wind direction, α_u the Kolmogorov constant) could be, in terms of natural frequency and the concept of surface layer similarity, rewritten as

$$\frac{f\,S_u(f)}{u_*^2}=\frac{\alpha_u}{(2\pi)^{2/3}}\frac{\varepsilon^{2/3}z^{2/3}}{u_*^2}\left(\frac{f\,z}{\bar{u}}\right)^{-2/3}=\frac{\alpha_u}{(2\pi)^{2/3}}\varphi_\varepsilon^{2/3}n^{-2/3}. \tag{17}$$

The Taylor hypothesis $k_1 = (2\pi f)/\bar{u}$ has also been used. Note that φ_ε in Eq.(17) is the universal similarity function of turbulence kinetic energe (TKE) dissipation rate presented in Eq. (9). Furthermore if we take $\alpha_u=0.50$ (see below), $k=0.40$, then Eq. (17) can be simplified to

$$\frac{f\,S_u(f)}{u_*^2\varphi_\varepsilon^{2/3}}=0.27n^{-2/3}. \tag{18}$$

Similarly the v, w and T spectra in inertial subrange can be derived:

$$\frac{f\,S_v(f)}{u_*^2\varphi_\varepsilon^{2/3}}=0.36n^{-2/3}, \tag{19}$$

$$\frac{f\,S_w(f)}{u_*^2\varphi_\varepsilon^{2/3}}=0.36n^{-2/3}, \tag{20}$$

$$\frac{f\,S_T(f)}{T_*^2\varphi_N\varphi_\varepsilon^{2/3}}=0.38n^{-2/3}, \tag{21}$$

where φ_N is the dissipation rate of non–dimensional temperature variance. With logarithmical plotting the spectra normalized in this way collapse into one straight line of slope $-2/3$ in the inertial subrange. Figs. 4—7 show a result quite consistent with Eqs. (18)—(21), respectively. In the non–dimensional spectrum calculations the following forms of φ_ε and φ_N have been adopted:

$$\varphi_\varepsilon=\varphi_m-z/L, \tag{22}$$

$$\varphi_N=\varphi_h, \tag{23}$$

where φ_m and φ_h took the widely–used Businger–Dyer profile–gradient relationships:

$$\varphi_m=\begin{cases}(1-16z/L)^{-1/4}, & (z/L\leqslant 0)\\ 1+5z/L, & (z/L>0)\end{cases} \tag{24}$$

$$\varphi_h=\begin{cases}(1-16z/L)^{-1/2}, & (z/L\leqslant 0)\\ 1+5z/L. & (z/L>0)\end{cases} \tag{25}$$

The stability range was from $z/L=-0.32$ to 0.31 for the runs plotted. The data points are most well–regulated in Fig. 4 in which with z/L increasing the spectral curves shift gradually to higher frequencies. As the variance analysis shown above, this also proves that the statistics of the vertical wind w agrees well with surface similarity. Comparatively, the spectra of horizontal wind u and v are different. In unstable air the spectral points of different runs tend to cluster in a random fashion. Turbulent energy occupied by their low frequency region is clearly higher than that of w–spectra, representing the effect of the higher altitude structure. Another feature of the Gobi u– and v–spectra is that in stable cases there are mostly two peaks clearly appearring in its low frequency region. Calculations by using of profile data show that the second peak is close to the Brunt–Vasala frequency, an effect of gravity waves induced by the local topography.

The form of temperature spectra is normally in between the vertical and horizontal wind spectra. Twin peaks are also clearly presented in stable conditions. This is consistent with Fig. 3 and the relevant analysis.

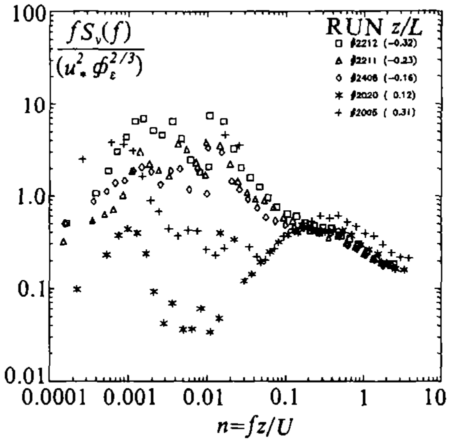

Fig. 4. Spectra of vertical wind component of 5 runs in different stabilities; Normalized by Kaimal scheme.

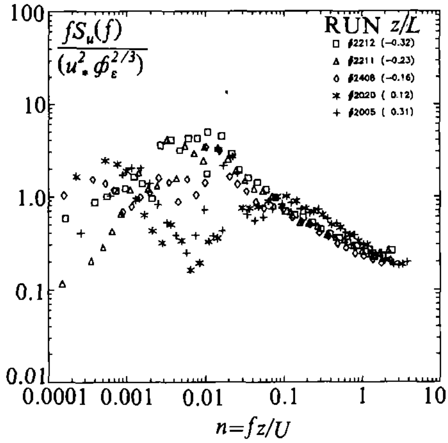

Fig. 5. As in Fig.4, but for along−wind component.

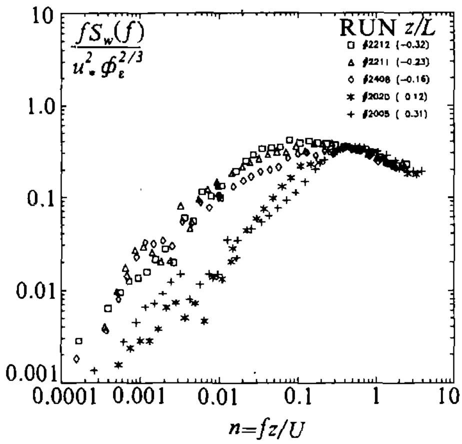

Fig. 6. As in Fig. 4, but for cross−wind component.

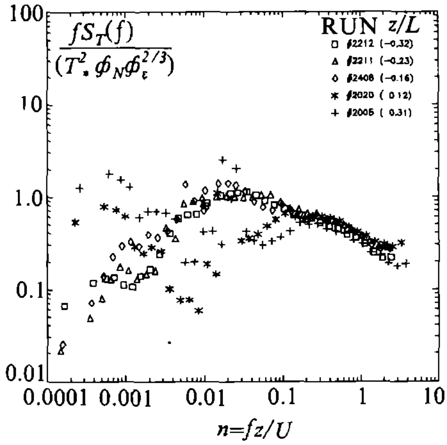

Fig. 7. Temperature spectra for the same runs as in Fig.4.

Other charateristics of turbulence spectra in the Gobi surface layer will be presented in another paper, including the variability of peak frequency with stability, the determination of Kolmogorov constants ($\alpha_u=0.50\pm0.04$, $\alpha_T=0.64\pm0.03$), the fitting form of φ_ε , etc. Generally speaking, the most features are rationally consistent with the results of horizontal surface experiments.

Figs. 8 and 9 show the cospectra of momentum ($\overline{u'w'}$) and temperature flux ($\overline{w'\theta'}$) of the same runs. Compared to power spectra, the collapse in both high and low frequency ends is obviously faster, and with a nearly $-3/4$ slope in the high frequencies. The frequency region of the latter coincides with the inertial subrange of the power spectra; this also shows that the large wave number turbulence is nearly in a state of local equilibrium, and with a very little contribution to the fluxes. The spectral collapse in both frequency ends for $\overline{u'w'}$ seems faster than that of $\overline{w'\theta'}$, i.e., the peak region of the cospectra of temperature flux is flatter than that of the momentum, but their frequency coverage is roughly the same. Cospectral analysis is helpful in determining the flux contribution of different eddy frequencies. It can be seen from the figures that in case of flux observation alone the sampling period can be shorter. Particularly in stable conditions, since more contribution is due to high frequency eddies, an average time of 15 to 20 minutes could be good respresentative in the calculation of heat and momentum fluxes.

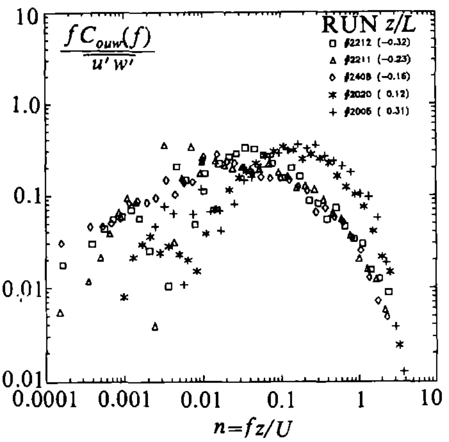

Fig. 8. Cospectra of momentum flux for the same runs as in Fig. 4.

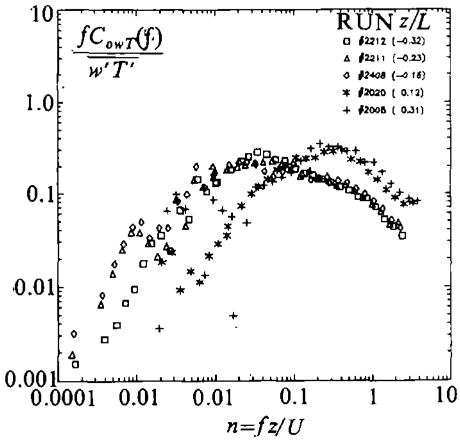

Fig. 9. Cospectra of sensible heat flux for the same runs as in Fig.4.

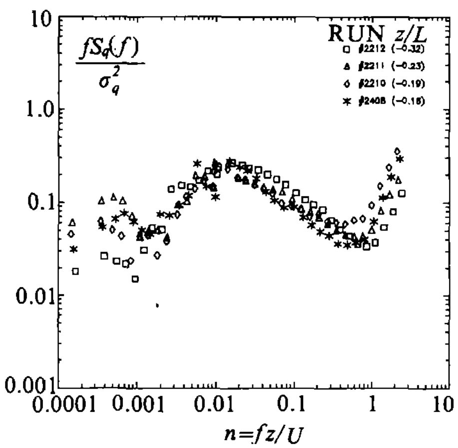

Fig. 10. Spectra of specific humidity (unstable cases).

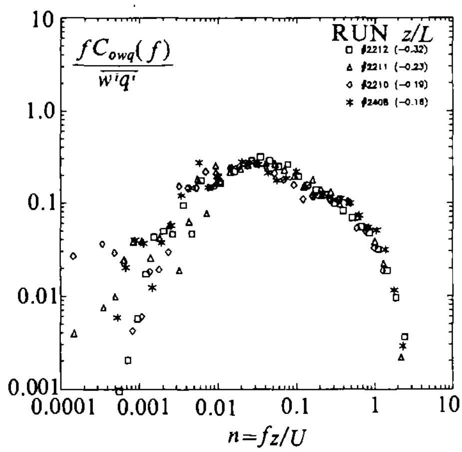

Fig. 11. Cospectra of water vapor flux for the same runs as in Fig. 10.

The spectrum of specific humidity derived from thermocouple psychrometer is normally with a larger scatter and bends upward in high frequency end, probably due to the time constant difference of its dry and wet bulb (about 0.19 s for dry bulb and 0.7 s for the wet). Although some compensation or correction has been adopted in the original data processing, matching imbalance could still exist at some frequencies, particularly in the high frequency end. Fig. 10 shows the q–spectra of four unstable runs. Their peak frequency $n \approx 0.01$, about the same of the temperature spectra. While $n > 1$, the spectrum curves bend up. However, as shown in Fig. 11, the cospectra of $\overline{w'q'}$ obviously drop down in this high frequency region, the bending up of the q–spectra does not mean a notable effect in the eddy–correlation calculations of the water vapor flux.

V. ENERGY BALANCE PROPERTY AND THE DOWNWARD WATER VAPOR FLUX IN DAYTIME

It was noticed in the Pilot Observation Period of 1988 that the water vapor flux in Gobi surface layer was mostly downward in daytime, as shown in Fig. 12 for the last seven days of the POP. The diurnal variations of net radiation (measured by radiometers) and sensible heat flux (by eddy–correlation method) were similar to many other observations; the sensible heat was comparatively larger in daytime, about 1 / 2 to 2 / 3 of the net radiation; Besides, there was a rather peculiar phenomenon: the latent heat, or water vapor flux, was nearly all negative in the day (0700—1900 LT), and changed to positive in late evening. The averaged downward vapor transportation in the day was about 12.4 g / m^2 per hour.

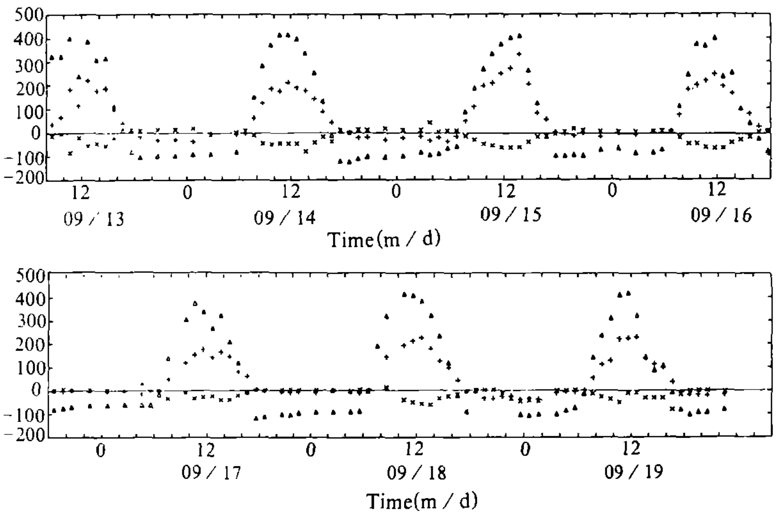

Fig. 12. Diurnal variation of net radiation (△), sensible heat (+), and latent heat (×), in 13—19 September 1988.

In the observation period of August 1990, there were slight or moderate rains several times. The phenomena of downward vapor transfer were not so obviously but still presented in more than half daytime runs. For the situation of dry weather lasted continuously several days, the diurnal variation of energy balance components was quite similar to that in Fig. 12. For instance, Fig. 13 shows the hourly variation of net radiation (*Rn*), sensible (*H*) and latent heat (*LE*), and ground heat flux (*G*, measured by heat flux plates at 5 cm deep) of August 20. The downward water vapor flux was confirmed by the profile measurements of specific humidity, as plotted in Fig. 14, the vertical profiles of humidity and temperature of 11 and 12 h of the same day. In the figure, humidity below 8 m (open circle) was measured by HUMICAP sensors on the tower, the upper layers by psychrometer of the TS–3A tethered–sondor. It is shown that there is no apparent humidity variation in the boundary layer below 500 m, however, for the lowest several observation levels the humidity 'inversion' is clearly presented for both tower and TS–3A measurements.

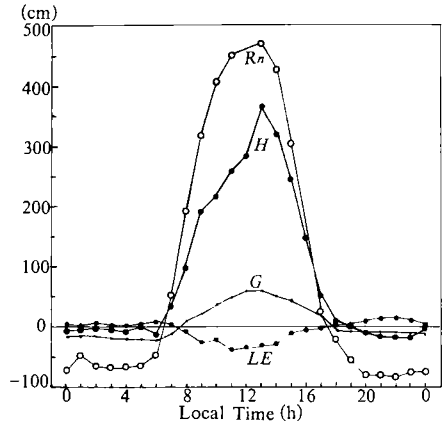

Fig. 13. Hourly variation of the surface layer energy budget components (Rn net radiation, H sensible heat, LE latent heat, G ground heat flux) in August 20, 1990, which is a clear day; in 0800 — 1800LT, the wind direction was mostly NNW and wind speed 4—7m / s; the wind reversed to S since 2000 LT and with a lower speed at night.

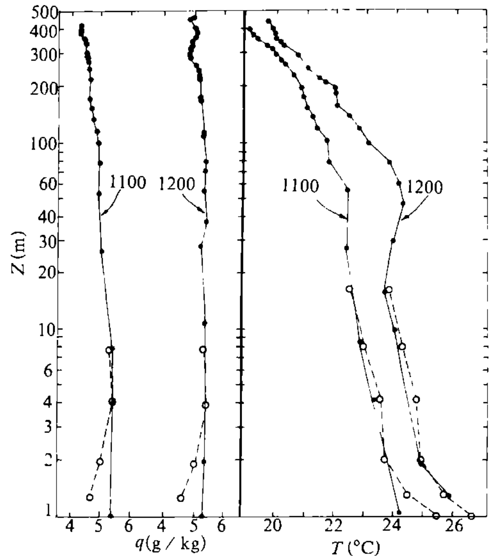

Fig. 14. Profiles of temperature (right) and specific humidity (left) at 11 and 12h, August 20, 1990. Open circles were measured by the tower, solid circle by tethered–sonde system.

This phenomenon, in fact, has also been noticed in some observational studies conducted in the same area a few years ago, and, in the 'Qinghai–Xizang (Tibet) Plateau Experiment' carried out in late 1970s. Only this time did we use more advanced equipment, so the phenomenon could be shown more clearly and quantitatively. A preliminary analysis indicates that the humidity inversion is closely related to a local mesoscale circulation, a mountain–valley wind system associated with the Qilian Mountain. The prevailing wind in the daytime is north to northwest, as cited in Fig. 13 for August 20. The humid air over the irrigated river basin oasis is advected to the Gobi desert. Therefore, in Gobi surface layer or to some height of the atmospheric boundary layer, the upper air would be more humid than the lower, and a downward water vapor flux would be formed. Because the Gobi surface in daytime is normally dry and hot, the downward water vapor would be absorbed, without phase changing, by the sand–pebble surface, and transferred to some depth in the ground by molecular and, probably, turbulent diffusion. The transfer depth is related to the soil structure and the larger humidity and temperature gradient under the Gobi surface.

At night the wind is normally reversed. The dry air from the north side of Qilian Mountain and the vast Gobi desert blows to this station. The water vapor absorbed by the sand soil in daytime could be formed to release to the air and formed a positive vapor flux.

Based on this analysis, the water vapor transfer normally does not join the energy balance process in Gobi surface layer, the latent heat in Figs. 12 and 13 only means vapor transfer. The three terms— net radiation, sensible heat, and ground heat flux are roughly in a balance as shown in Fig. 13.

The phenomenon of downward water vapor flux over Gobi desert in the daytime, in fact, is the another side of the well–known oasis effect. In daytime over oasis the air in the lower level is often rather wet and cool, the higher level rather dry and hot. The water vapor transfers upwards, while the sensible heat transfers downwards. This is just the opposite to the Gobi situation. Moreover, sometimes the measured latent heat over oasis is even larger than net radiation because the surface extracts more energy from the warmer air.

VI. CONCLUSION

In September of 1988 and August of 1990, two observational experiments have been carried out in the HEIFE Gobi Station. A data set on the surface layer turbulence has been collected, which is proved to be of high quality. An analysis on the surface layer structure shows that turbulence statistics such as the variances of vertical wind component and temperature are in good agreement with the surface layer similarity theory; the relevant forms of similarity function are presented. The characteristics of the power spectra of wind components, temperature, and humidity, and the cospectra of momentum and sensible heat flux are similar to that of flat and horizontal terrain. For the spectra of horizontal wind the low frequency region shows large scatter in unstable stratification and two apparent peaks in stable cases. The phenomenon of downward water vapor flux over Gobi desert in the daytime, which was clearly noticed in 1988, is confirmed in the PIOP of 1990. An analysis on its physical mechanism is given in Section V. As the well–known oasis effect, this phenomenon is closely related to a local "Gobi desert–oasis" circulation system. It is also proved through these two pilot observational studies that our turbulence data acquisition system works satisfactorily, the relevant real–time data processing software is also well–done; this forms a good basis for the formal HEIFE experiment.

REFERENCES

Grant, A. L. M. and Watkins, R. D. (1989), Errors in turbulence measurements with a sonic anemometer, *Boundary–Layer Meteor.*, **46**:181—189.

Hogstrom, U. (1990), Analysis of turbulence structure in the surface layer with a modified similarity formulation for near neutral conditions, *J. Atm. Sci.*, **47**:1949—1972.

Kaimal, J. C., Wyngaard, J. C., Izumi, Y. and Cote, O. R. (1972), Spectral characteristics of surface layer turbulence, *Q. J. Roy. Meteor. Soc.*, **98**:563—589.

Panofsky, H. A. and Dutton, J. A.(1984), *Atmospheric Turbulence*, John Wiley & Sons, New York, 397pp.

Shao, Y. and Hacker, J. M. (1990), Local similarity relationship in a horizontally inhomogeneous boundary layer, *Boundry–Layer Meteor.*, **52**:41—68.

Tsukmoto, O. (1986), Dynamic response of the fine wire psychometer for direct measurement of water vapor flux, *J.*

Atm. Ocean Technology, **3**:453—461.

Wang Jiemin, Liu Xiaohu and Qi Yongqiang (1990), A preliminary study of turbulence transfer characteristics over Gobi desert, *Plateau Meteor.*, **9**:120—129 (in Chinese).

Wyngaard, J. C. (1973), On surface layer turbulence, in *Workshop in Micrimeteorology*, AMS, Boston, MA, pp.101—149.